

**GROUND PENETRATING RADAR:  
ANALYSIS OF POINT DIFFRACTORS FOR MODELING  
AND INVERSION**

**Albane Saintenoy**

*Colorado School of Mines, Department of Geophysics, Golden CO 80403, USA*

**Albert Tarantola**

*Institut de Physique du Globe, 4, place Jussieu, 75252 Paris Cedex 05, France*

(January 20, 1999)

**ABSTRACT**

The three electromagnetic properties appearing in Maxwell's equations are the electric permittivity, the electric conductivity and the magnetic permeability. The study of point diffractors in an homogeneous, isotropic, and linear medium suggests the use of logarithms to describe the variations of electromagnetic properties in the earth. A small anomaly in electric properties (permittivity and conductivity) responds to an incident electromagnetic field as an electric dipole, whereas a small anomaly in the magnetic property responds as a magnetic dipole. No property variation can be neglected compared to the others. Furthermore, considering radiation patterns of the different diffraction points, differentiating electric and magnetic variations is not an easy task using Ground Penetrating Radar. But using an effective electromagnetic impedance and an effective electromagnetic velocity to describe a medium, the corresponding radiation patterns behave completely differently with the source-receiver

offset. Zero-offset reflection data give a direct image of impedance variations with depth while large-offset reflection data contain information on velocity variations.

## INTRODUCTION

Ground Penetrating Radar (GPR) should yield information on the electric and magnetic properties of a medium at small scales (from a few centimeters for a 900 MHz antenna to a few meters for a 50 MHz antenna). A key issue for this paper is to find a good parameterization of the subsurface for the inverse problem, taking into account some earth media containing high permeability perturbations (metallic object, magnetite, iron-bearing rocks,...).

For instance, it is now well understood (Tarantola, 1986; Dębski and Tarantola, 1995) that using multi-offset seismic data, from the three parameters necessary to describe an elastic medium, one can resolve, in order of importance, the acoustic impedance contrasts (controlling the reflection amplitude at small offsets), the contrasts in Poisson's ratio (controlling the variation of reflection amplitude as a function of offset), and the contrasts in mass density (this parameter being very poorly resolved). These elastic parameters are nonlinear combinations of the parameters appearing explicitly in the elastic wave equation (the Lamé parameters).

When we started the present research, it was not obvious which functions of the three electromagnetic parameters (electric permittivity, electric conductivity, and magnetic permeability) could be resolved using GPR data. Following the seismic approach (Tarantola, 1986), we will show below that the effective electromagnetic impedance and the effective electromagnetic velocity can be resolved separately from GPR data.

On the other hand, modeling of GPR data requires the solution of Maxwell's equations. One approach is to linearize Maxwell's equations by approximating the medium as a superposition of diffraction points superimposed on a smooth surround-

ing medium. Here we consider a single point diffractor behavior in an isotropic, linear, non-dispersive and homogeneous surrounding medium submitted to a propagating electromagnetic wave.

## POINT DIFFRACTORS

### Logarithmic parameters

GPR sends an electromagnetic wave into the ground and measures the returning field amplitude. This electromagnetic wave consists of a pair of electromagnetic fields ( $\mathbf{E}, \mathbf{B}$ ). We consider, as an external source, a density of currents  $\mathbf{J}_s$  (e.g. a bow-tie antenna). Currents inside the medium result from polarization and conduction (Ohm's law). Electromagnetic fields in an isotropic (parameters are scalar and not tensors), linear and non-dispersive (parameters do not depend on time) medium, are governed by Maxwell's equations (Jackson, 1975), summed up in the MKSA system as

$$\nabla \cdot (\varepsilon(\mathbf{x})\mathbf{E}(\mathbf{x}, t)) = \rho(\mathbf{x}, t), \quad (1)$$

$$\nabla \times \left( \frac{\mathbf{B}(\mathbf{x}, t)}{\mu(\mathbf{x})} \right) - \varepsilon(\mathbf{x}) \frac{\partial}{\partial t} \mathbf{E}(\mathbf{x}, t) - \sigma(\mathbf{x}) \mathbf{E}(\mathbf{x}, t) = \mathbf{J}_s(\mathbf{x}, t), \quad (2)$$

$$\nabla \cdot \left( \frac{\mathbf{B}(\mathbf{x}, t)}{\mu(\mathbf{x})} \right) = 0, \quad (3)$$

$$\nabla \times \mathbf{E}(\mathbf{x}, t) + \frac{\partial}{\partial t} \mathbf{B}(\mathbf{x}, t) = \mathbf{0}, \quad (4)$$

where  $\nabla$  is the Nabla operator,  $\mathbf{x}$  the spatial position,  $t$  is time,  $\rho$  is the density of electric charges and  $\times$  indicates the cross product.

The parameters appearing in these equations are the electric permittivity  $\varepsilon$ , the electric conductivity  $\sigma$ , and the magnetic permeability  $\mu$  which are positive. From

the literature (Olhoeft, 1979; Olhoeft and Capron, 1993; Schön, 1996), it is known that for earth material

$$\left\{ \begin{array}{l} \varepsilon_0 \leq \varepsilon \leq 100 \varepsilon_0, \\ 10^{-7} < \sigma \leq 10^7, \\ (1 - 10^{-4})\mu_0 \leq \mu \leq 100 \mu_0. \end{array} \right. \quad (5)$$

The reason why the electric permittivity is always greater than  $\varepsilon_0$ , the electric permittivity of vacuum, is explained by Landau and Lifshitz (1960) from thermodynamics considerations. Rocks presenting exclusively diamagnetic properties are characterized by a magnetic permeability lower than  $\mu_0$ , the magnetic permeability in vacuum. The inequalities (5) allows one to define the logarithmic parameters  $\varepsilon^*$ ,  $\sigma^*$  and  $\mu^*$  (logarithm of the linear parameter over an arbitrarily chosen reference value),

$$\begin{aligned} \varepsilon^* &= \ln \left( \frac{\varepsilon}{\varepsilon_0} \right), \\ \sigma^* &= \ln \left( \frac{\sigma}{\sigma_0} \right), \\ \mu^* &= \ln \left( \frac{\mu}{\mu_0} \right), \end{aligned} \quad (6)$$

where  $\sigma_0$  is chosen equal to 1 S/m. Furthermore, in earth material, lognormal statistics describe the electromagnetic property variations (Saintenoy, 1998).

We will consider time-independent contrasts in these logarithmic parameters and assess their implication in GPR data, depending on the frequency and the acquisition geometry.

### **Diffracted field using $(\varepsilon, \sigma, \mu)$ parameterization**

Small perturbations  $\delta\varepsilon$ ,  $\delta\sigma$  and  $\delta\mu$ , in electromagnetic parameters of a homogeneous, linear, non-dispersive and isotropic medium described by  $\varepsilon$ ,  $\sigma$  and  $\mu$ , can be

written as

$$\begin{aligned}
\varepsilon \text{ becomes } \varepsilon + \delta\varepsilon &= \varepsilon \exp \delta\varepsilon^* \approx \varepsilon(1 + \delta\varepsilon^*), \\
\sigma \text{ becomes } \sigma + \delta\sigma &= \sigma \exp \delta\sigma^* \approx \sigma(1 + \delta\sigma^*), \\
\mu \text{ becomes } \mu + \delta\mu &= \mu \exp \delta\mu^* \approx \mu(1 + \delta\mu^*),
\end{aligned} \tag{7}$$

where  $\delta m^*$  is the logarithmic parameter variation of  $m^*$ ,  $m$  being either  $\varepsilon$ ,  $\sigma$  or  $\mu$ .

Then

$$\delta m^* = (m + \delta m)^* - m^* = \ln \frac{m + \delta m}{m_0} - \ln \frac{m}{m_0} = \ln \frac{m + \delta m}{m}. \tag{8}$$

Linearization of equations (7) suggests to use relative variations instead of absolute variations compared with the surrounding medium.

Taking into account these perturbed parameters, equation (2) yields (after canceling the background terms and keeping only first order terms)

$$\begin{aligned}
\nabla \times \left( \frac{\delta \mathbf{B}(\mathbf{x}, t)}{\mu} \right) - \varepsilon \frac{\partial}{\partial t} \delta \mathbf{E}(\mathbf{x}, t) - \sigma \delta \mathbf{E}(\mathbf{x}, t) = \\
\nabla \times \left( \frac{\delta \mu^*(\mathbf{x})}{\mu} \mathbf{B}(\mathbf{x}, t) \right) + \varepsilon \delta \varepsilon^*(\mathbf{x}) \frac{\partial}{\partial t} \mathbf{E}(\mathbf{x}, t) + \sigma \delta \sigma^*(\mathbf{x}) \mathbf{E}(\mathbf{x}, t).
\end{aligned} \tag{9}$$

It is as if the perturbed fields  $\delta \mathbf{E}$  and  $\delta \mathbf{B}$  propagate in the non perturbed medium described by parameters  $\varepsilon$ ,  $\sigma$  and  $\mu$ , with some electric sources (terms on the right side in equation (9)) depending on logarithmic parameter variations and the electromagnetic field  $\mathbf{E}$  and  $\mathbf{B}$  that would have existed if there was no perturbation.

When the perturbation in parameters at point  $\mathbf{x}_0$  can be written as,

$$\begin{cases} \delta \varepsilon^*(\mathbf{x}) = A_\varepsilon^* \delta(\mathbf{x} - \mathbf{x}_0) \\ \delta \sigma^*(\mathbf{x}) = A_\sigma^* \delta(\mathbf{x} - \mathbf{x}_0) \\ \delta \mu^*(\mathbf{x}) = A_\mu^* \delta(\mathbf{x} - \mathbf{x}_0), \end{cases} \tag{10}$$

the corresponding diffraction point anomaly acts as a localized point source.  $A_\varepsilon^*$  is a perturbation in logarithmic permittivity (which tends to infinity) multiplied by

the perturbation volume (which tends to zero). It is the same for  $A_\sigma^*$  and  $A_\mu^*$  with, respectively, the logarithmic conductivity and the logarithmic permeability.  $\delta(\mathbf{x} - \mathbf{x}_0)$  is the Dirac function.

We want to know the characteristics of the electric field diffracted by such a localized point source. The answer for a homogeneous, isotropic, non-dispersive and linear medium to an electric current density source  $\mathbf{J}_s$  is given by the solution of the equation

$$\nabla\nabla \cdot \mathbf{E}(\mathbf{x}, t) - \nabla^2 \mathbf{E}(\mathbf{x}, t) - \mu\varepsilon \frac{\partial^2}{\partial t^2} \mathbf{E}(\mathbf{x}, t) + \mu\sigma \frac{\partial}{\partial t} \mathbf{E}(\mathbf{x}, t) = -\mu \frac{\partial}{\partial t} \mathbf{J}_s(\mathbf{x}, t). \quad (11)$$

This equation is the rotational of equation (4) combined with the time derivative of equation (2) when  $\mathbf{J}_s(\mathbf{x}, t) = \mathbf{J}(t)\delta(\mathbf{x} - \mathbf{x}_0)$ , with  $\mathbf{J}$  a density of currents independent of space position. The solution of equation (11) is a Green tensor. When the medium has small conductivity ( $\sigma \ll \varepsilon\omega$  where  $\omega$  is the frequency), the far-field term of the Green tensor is written in the space-time domain (de Hoop (1995) and others) as

$$G^{ij}(\mathbf{x}, t, \mathbf{x}_0, t_0) = \frac{1}{4\pi r} (\delta^{ij} - \gamma^i \gamma^j) \delta(t - t_0 - \frac{r}{c}), \quad (12)$$

where  $r = \|\mathbf{x} - \mathbf{x}_0\|$  is the distance to the origin (the source position),  $c = \sqrt{1/\mu\varepsilon}$  is the electromagnetic velocity, and  $\gamma^i = (x^i - x_0^i)/r$  are the direction cosines pointing to point  $\mathbf{x}$  from the origin  $\mathbf{x}_0$ .

The  $i$ -th component of the far-field diffracted by some more general source  $\mathbf{J}_s(\mathbf{x}, t)$  localized at  $\mathbf{x}_0$ , in a surrounding linear, isotropic, homogeneous, non-dispersive and low-conductive medium is

$$\delta E^i(\mathbf{x}, t) = G^{ij}(\mathbf{x}, t, \mathbf{x}_0, t_0) * \mu \frac{\partial}{\partial t} J_s^j(\mathbf{x}_0, t_0), \quad (13)$$

with an implicit summation on the repeated indices and with a time-convolution represented by a star (\*).

When the conductivity is not negligible compared to  $\varepsilon\omega$ , the diffracted field will arrive at a given receiver more or less delayed and amplified than the one given by

equation (13). But these differences will not depend on the logarithmic parameter variations in themselves. An actual computation of the amplitudes received at the surface using GPR should take into account the diffraction patterns here investigated and the amplitude losses, as well as the signal dispersion. Here we are concerned with the differentiation between the effect on the electric field of each kind of parameter anomaly in a homogeneous surrounding medium. Not with the surrounding medium properties. This is why we consider a homogeneous, isotropic, low-conductive and non-dispersive medium.

Furthermore, only the far-field is considered here because we are interested in the field diffracted back to the surface and it is assumed that the near field term (decreasing as  $\frac{1}{r^3}$ ) will be negligible at this distance.

The field  $\delta\mathbf{E}$  diffracted by a small perturbation in electromagnetic parameters is calculated (Saintenoy, 1998) from equation (13), with equation (4),

$$\begin{aligned} \delta\mathbf{E}(\mathbf{x}, t) = & \frac{1}{4\pi r c^2} \left[ A_\varepsilon^* \left( \mathbf{r} \times \frac{\partial^2}{\partial t^2} \mathbf{E} \left( \mathbf{x}_0, t - \frac{r}{c} \right) \right) \times \mathbf{r} \right. \\ & + \mu\sigma c^2 A_\sigma^* \left( \mathbf{r} \times \frac{\partial}{\partial t} \mathbf{E} \left( \mathbf{x}_0, t - \frac{r}{c} \right) \right) \times \mathbf{r} \\ & \left. + A_\mu^* \left( \mathbf{R}_{inc} \times \frac{\partial^2}{\partial t^2} \mathbf{E} \left( \mathbf{x}_0, t - \frac{r}{c} \right) \right) \times \mathbf{r} \right], \end{aligned} \quad (14)$$

where  $\mathbf{r}$  is the unit vector pointing from the diffracting point  $\mathbf{x}_0$  to the observation point  $\mathbf{x}$ .  $\mathbf{R}_{inc}$  is the unit vector in direction of the incident wavefront displacement (Figure 1). The diffracted magnetic field associated with the diffracted electric field is given by equation (4).

The analytical expression (14) of the diffracted electric field allows one to separate the contribution of each kind of anomaly to the total diffracted field. A point anomaly in a surrounding medium described by non-zero parameters diffracts an electric field  $\delta\mathbf{E}$  that is the sum of three terms. In each term, the amplitude of  $\delta\mathbf{E}$  is proportional to the contrasts  $A_\varepsilon^*$ ,  $A_\sigma^*$  or  $A_\mu^*$ , with a given spatial dependence (cross products between  $\mathbf{r}$  and the incident electric field  $\mathbf{E}$ ) and a given time dependence (first or

second time derivative of the incident electric field  $\mathbf{E}$ ). The contribution to  $\mathbf{E}$  due to electric permittivity contrasts  $A_\epsilon^*$  has the same spatial dependence as the contribution due to electric conductivity contrasts  $A_\sigma^*$ , but not the same time dependence. The distribution of the diffracted field amplitude over a sphere centered on the point anomaly is called a radiation pattern. To have the same spatial dependence means to have the same radiation pattern. Therefore, an anomaly in electric permittivity  $A_\epsilon^*$  alone has the same radiation pattern as an anomaly in electric conductivity  $A_\sigma^*$  alone, but not as an anomaly in magnetic permeability  $A_\mu^*$  alone. This justifies the consideration of only two kind of diffraction points: the electric diffraction point and the magnetic diffraction point.

Note that a point anomaly in vacuum diffracts an electric field. But there will be no contribution from the electric conductivity to this diffracted field as  $\sigma = 0$  in vacuum.

### **Radiation and polarization patterns**

Each kind of diffraction point is described by a radiation pattern and a polarization pattern (display of the diffracted electric field with its polarization and its amplitude over a sphere centered on the point anomaly). Figure 2 displays those two patterns for an electric diffraction point. The radiation pattern (left) is a torus centered on the point anomaly and with a zero radius central circle. No electric field is diffracted in the direction of electric incident field (axis of the torus). The polarization pattern (right) shows that the diffracted electric fields is poloidal, whereas the magnetic diffracted field is toroidal. Those patterns are the same obtained in the far-field for a small electric dipole submitted to an incident electromagnetic field (the axis of the dipole being in the same axis as the electric incident field).

On the other hand, a magnetic diffraction point reacts in the far-field as a small magnetic dipole when submitted to an electromagnetic field. That is to say, the

magnetic diffracted field is the same as the electric field diffracted by a small electric dipole parallel to the magnetic incident field. Then the magnetic field diffracted by a magnetic diffraction point is poloidal, whereas the electric diffracted field is toroidal. The polarization pattern is displayed on the right of Figure 3. This figure displays also on the left the radiation pattern, a torus perpendicular to the torus on Figure 2.

### Point diffractor in $(\varepsilon_e, \mu)$ and $(Z, c)$ parameterization

A point contrast in electric conductivity diffracts an electromagnetic field with the same radiation pattern as a point contrast in electric permittivity. But the field diffracted by the conductivity contrast alone depends on the first-time derivative of the incident electric field whereas the field diffracted by the permittivity contrast alone depends on the second-time derivative of the electric incident field. Electric permittivity and conductivity are merged into the effective electric permittivity  $\varepsilon_e$ ,

$$\varepsilon_e \delta(t) = \varepsilon \delta(t) + \sigma H(t), \quad (15)$$

where  $H(t)$  is the Heaviside function. In the Fourier domain, the effective electric permittivity (Jackson [1975] and others) is

$$\varepsilon_e = \varepsilon + \frac{\sigma}{i\omega}, \quad (16)$$

where  $i^2 = -1$  and  $\omega$  is the incident field frequency. Equation (2) becomes

$$\nabla \times \left( \frac{\mathbf{B}(\mathbf{x}, t)}{\mu(\mathbf{x})} \right) - \varepsilon_e(\mathbf{x}) * \frac{\partial}{\partial t} \mathbf{E}(\mathbf{x}, t) = \mathbf{J}_s(\mathbf{x}, t), \quad (17)$$

where  $*$  represents a time convolution.

Following the same approach set forth in this paper, we show that a small perturbation in logarithmic effective permittivity, submitted to an incident electromagnetic field, acts as a secondary source of current density,

$$\mathbf{J}_s(\mathbf{x}, t) = \varepsilon_e(\mathbf{x}) \delta \varepsilon_e^*(\mathbf{x}) * \frac{\partial}{\partial t} \mathbf{E}(\mathbf{x}, t). \quad (18)$$

A point anomaly that is described by

$$\begin{cases} \delta\varepsilon_e^*(\mathbf{x}) = A_{eff}^* \delta(\mathbf{x} - \mathbf{x}_0) \\ \delta\mu^*(\mathbf{x}) = A_\mu^* \delta(\mathbf{x} - \mathbf{x}_0), \end{cases} \quad (19)$$

in a surrounding isotropic, homogeneous, linear, non-dispersive, and low-conductive medium diffracts an electric field (Saintenoy, 1998)

$$\begin{aligned} \delta\mathbf{E}(\mathbf{x}, t) = \frac{\varepsilon\mu}{4\pi r} & \left[ A_{eff}^* * \left( \mathbf{r} \times \frac{\partial^2}{\partial t^2} \mathbf{E} \left( \mathbf{x}_0, t - \frac{r}{c} \right) \right) \times \mathbf{r} \right. \\ & \left. + A_\mu^* \left( \mathbf{r}_{inc} \times \frac{\partial^2}{\partial t^2} \mathbf{E} \left( \mathbf{x}_0, t - \frac{r}{c} \right) \right) \times \mathbf{r} \right]. \end{aligned} \quad (20)$$

$A_{eff}^*$  and  $A_\mu^*$  are the perturbations in logarithmic parameters multiplied by the volume of the anomaly.

The effective impedance  $Z$  and the effective velocity  $c$  are defined from the magnetic permeability and the effective electrical permittivity as

$$Z = \sqrt{\frac{\mu}{\varepsilon_e}}, \quad (21)$$

$$c = \sqrt{\frac{1}{\mu\varepsilon_e}}. \quad (22)$$

Then

$$A_Z^* = \frac{1}{2}(A_\mu^* - A_{eff}^*), \quad (23)$$

$$A_c^* = \frac{1}{2}(-A_\mu^* - A_{eff}^*), \quad (24)$$

and using those parameters, equation (20) becomes (Saintenoy, 1998)

$$\begin{aligned} \delta\mathbf{E}(\mathbf{x}, t) = \frac{\varepsilon\mu}{4\pi r} & \left[ A_Z^* * \left( (-\mathbf{r} + \mathbf{r}_{inc}) \times \frac{\partial^2}{\partial t^2} \mathbf{E} \left( \mathbf{x}_0, t - \frac{r}{c} \right) \right) \times \mathbf{r} \right. \\ & \left. - A_c^* * \left( (\mathbf{r} + \mathbf{r}_{inc}) \times \frac{\partial^2}{\partial t^2} \mathbf{E} \left( \mathbf{x}_0, t - \frac{r}{c} \right) \right) \times \mathbf{r} \right]. \end{aligned} \quad (25)$$

$A_Z^*$  and  $A_c^*$  are the perturbations in logarithmic parameters multiplied by the volume of the anomaly. Derived from equation (25), the radiation and polarization patterns associated with a point diffractor described by the parameters  $Z$  and  $c$  are displayed in Figures 4 and 5.

## DISCUSSION

### Importance of each parameter in the $(\varepsilon, \sigma, \mu)$ set

The expression of the diffracted field in equation (14) allows us to compare the relative importance of contrasts in the three parameters,  $\varepsilon$ ,  $\sigma$  and  $\mu$ . The maximum amplitude of the field diffracted by an electric permittivity anomaly is

$$|\delta \mathbf{E}|_{\varepsilon} = \frac{1}{4\pi r c^2} A_{\varepsilon}^* \omega^2 |\mathbf{E}|, \quad (26)$$

by an electric conductivity anomaly,

$$|\delta \mathbf{E}|_{\sigma} = \frac{1}{4\pi r} \mu \sigma A_{\sigma}^* \omega |\mathbf{E}|, \quad (27)$$

and by magnetic permeability anomaly,

$$|\delta \mathbf{E}|_{\mu} = \frac{1}{4\pi r c^2} A_{\mu}^* \omega^2 |\mathbf{E}|, \quad (28)$$

with  $A_m^* = V_a \ln \frac{m_a}{m}$ , where  $m$  is  $\varepsilon$ ,  $\sigma$  or  $\mu$ ,  $m_a$  is the parameter value in the anomaly,  $V_a$  is the anomaly volume, and  $\omega$  the incident wave frequency. The contribution of each parameter is then proportional to  $\varepsilon A_{\varepsilon}^* \omega$ ,  $\sigma A_{\sigma}^*$  and  $\varepsilon A_{\mu}^* \omega$ .

Consider a small volume composed of a mixture of -400 mesh iron filings in homogeneous dry sand, subjected to an electromagnetic field of central frequency 600 MHz. Realistic parameter values for mesh iron  $(\varepsilon_a, \sigma_a, \mu_a)$  and dry sand  $(\varepsilon, \sigma, \mu)$  can be found in Olhoeft and Capron's report (1993),

$$\begin{aligned} \varepsilon &= 5\varepsilon_0, & \varepsilon_a &= 18\varepsilon_0, \\ \mu &= \mu_0, & \mu_a &= 4\mu_0, \\ \sigma &= 10^{-3} \text{ S/m}, & \sigma_a &= 10 \text{ S/m}. \end{aligned}$$

Then,

$$\varepsilon \ln \frac{\varepsilon_a}{\varepsilon} \omega \approx 3.40 \cdot 10^{-2} \text{ S/m}$$

for the electric permittivity contrast contribution,

$$\sigma \ln \frac{\sigma_a}{\sigma} \approx 0.92 \cdot 10^{-2} \text{ S/m}$$

for the electric conductivity contrast contribution, and

$$\varepsilon \ln \frac{\mu_a}{\mu} \omega \approx 3.68 \cdot 10^{-2} \text{ S/m}$$

for the magnetic permeability contrast contribution.

In our example, the three contributions to the total diffracted field are of the same order of magnitude. Terms in front of electric permittivity and magnetic permeability contrasts are proportional to  $\omega$  while the electric conductivity contrast contribution does not depend on  $\omega$ . So electric permittivity and magnetic permeability contrasts contributions would dominate in an experiment using a higher central frequency. However, the permeability contrasts contribution to the amplitude of the total diffracted field can not be neglected in comparison to the permittivity contrast contribution. Lázaro-Mancilla et al. (1996) find the same result but think that the magnetic permeability does not vary a lot in most of the studied earth material. On the other hand, metals, magnetite, gneiss or quartzite have relative permeability value that differ significantly of 1.

### **New geometry of acquisition ?**

From equation (14), the radiation and polarization patterns associated with contrasts in each parameter are known and displayed on Figures 2 and 3. Figures 6 and 7 sum up the same information on radiation and polarization, each displaying three views. They show the effects of different geometries of acquisition. The fields diffracted by a point anomaly recorded with zero-offset measurements are read in the middle of the view from the top side (xy). Magnetic and electric effects are then indistinct.

An acquisition using two radar antennae parallel to each other and perpendicular to the acquisition profile consists of recording the diffracted field along the x axis. On the (xy) view of Figure 6, the amplitude of the diffracted field is constant with the offset whereas it is decreasing with the offset on the (xy) view of Figure 7. Therefore, the electric behavior is different from the magnetic behavior. For a magnetic anomaly, the amplitude of the diffracted field depends on the offset, while for an electric anomaly it does not.

When using two radar antennae parallel to each other and parallel to the acquisition profile, the field diffracted by an anomaly is recorded along the y axis. On the (xy) view of Figure 6, the amplitude of the diffracted field decreases with the offset whereas it is constant with the offset on the (xy) view of Figure 7. Then, the amplitude depends on the offset for an electric anomaly, while for a magnetic anomaly it does not.

Another interesting acquisition of data would be using the source antenna at 45 degrees from the profile direction. The result of this experiment can be seen along an axis at 45 degrees of x and y axis, on (xy) views of Figures 6 and 7. The electric field diffracted by an electric point anomaly is not in the same direction as the one diffracted by a magnetic point anomaly. It shows that multi-component measurements can, in this case, distinguish magnetic from electrical effects. But such observations are not easy to obtain in real experiments with current GPR due to the uncertainty of antennae directivity.

### **The inversion parameters: $Z$ and $c$**

Because of the difficulty of separating magnetic effect from electrical effect,  $Z$  and  $c$  will be the keys to the inverse problem. From Figures 4 and 5, one can see that zero-offset data are governed by the variations of the electromagnetic impedance alone, whereas large-offset data contain information on the effective velocity.

To illustrate how parameterizing with  $Z$  and  $c$  contributes to the inverse problem, consider the case of a small (volume of  $0.00052\text{m}^3$ ) iron-bearing sand anomaly ( $\epsilon_a^* = 2.1$ ,  $\mu_a^* = 1$  and  $\sigma_a^* = -2.3$ ) at two meters deep in dry sand ( $\epsilon^* = 1.6$ ,  $\mu^* = 0$  and  $\sigma^* = -4.6$ ). Supposing the use of 600 MHz antennae in Common Mid Point gather (the two antennae move symmetrically away from each other starting from the vertical of the point diffractor), the recorded signal at the receiver is simulated on Figure 9. The example takes into account the radiation pattern of source and receiver antennae shown on Figure 8. Peak to peak amplitudes are represented in Figure 10. Independently from the antennae radiation pattern, this simulation shows that the electric field recorded at zero offset depends only on the effective impedance contrast. And in this example, the effective velocity contrast contribution predominates for offsets larger than 360 cm.

## CONCLUSIONS

In this paper we have studied a point diffractor in a homogeneous, linear, isotropic, low-conductive and non-dispersive medium, using different parameterizations. Logarithmic electric permittivity anomalies behave similarly to those of logarithmic electric conductivity alone. This statement is not surprising as it is well-known that permittivity and conductivity are merged into a single parameter, the effective permittivity, used to describe the electric properties of a medium. But, by considering permittivity and conductivity separately we see that electric conductivity perturbations alone do not dominate electric permittivity perturbations or magnetic permeability perturbations alone.

Furthermore, in the far field approximation, a point logarithmic effective electric permittivity anomaly acts as a small electric dipole. A point logarithmic effective magnetic permeability anomaly acts as a small magnetic dipole. These two behaviors are not identical. Electric and magnetic effects could be differentiated with GPR

surface data, playing with antennae orientation. But, if instead of parameterizing a medium with electric and magnetic parameters, we use its effective electromagnetic impedance and its effective electromagnetic velocity, the point diffractor study raises some new elements. Radiation patterns show that the effective impedance controls the amplitude reflected at small offsets, whereas the effective velocity controls the amplitude reflected at large offset.

A multi-offset data acquisition allows a multi-parameter measurement. A radar image obtained in monostatic mode is a direct image of the effective impedance contrasts. A radar image obtained with a large offset between the source and the receiver contains information about effective velocity contrasts.

#### **ACKNOWLEDGMENTS**

This work was supported by the Bureau de Recherche Géologique et Minière (Orléans) and done in the Département de Sismologie de l'Institut Physique du Globe de Paris. The comments and suggestions of several Colorado School of Mines faculty are also gratefully acknowledged.

#### **REFERENCES**

- Dębski, W., and Tarantola, A., 1995, Information on elastic parameters obtained from amplitude of reflected waves: *Geophysics*, **60**, no. 5, 1426–1436.
- de Hoop, A. T., 1995, *Radiation and scattering of waves*: Academic Press.
- Jackson, J. D., 1975, *Classical electrodynamics*: John Wiley & Sons, 2 edition.
- Landau, L., and Lifshitz, E., 1960, *Electrodynamics of continuous media*: Addison-Wesley.

- Lázaro-Mancilla, O., and no, E. G.-T., 1996, Synthetic radargrams from electrical conductivity and magnetic permeability variations: *Applied Geophysics*, **34**, 283–290.
- Olhoeft, G. R., and Capron, D. E., Laboratory measurements of the radiofrequency electrical and magnetic properties of soils from near yuma, arizona:, Open File Report 93-701, U. S. Geological Survey, 1993.
- Olhoeft, G., Tables of room temperature electrical properties for selected rocks and minerals with dielectric permittivity statistics:, Open File Report 79-993, U. S. Geological Survey, 1979.
- Saintenoy, A., 1998, Radar géologique : acquisition multi-déports pour une mesure multi-paramètres: Ph.D. thesis, Paris 7.
- Schön, J. H., 1996, Physical properties of rocks: fundamentals and principles of petrophysics: Pergamon.
- Tarantola, A., 1986, A strategy for nonlinear elastic inversion of seismic reflection data: *Geophysics*, **51**, no. 10, 1893–1903.

## FIGURES

FIG. 1. Position of the antennae and polarization of incident electromagnetic fields on point P.

FIG. 2. Radiation and polarization diagrams of an electric dipole, i.e., intensity, direction, and sense of the field diffracted by a point anomaly in electric permittivity alone, or, electric conductivity alone when illuminated by an electromagnetic wave moving in the  $R_{inc}$  direction with an electric field  $\mathbf{E}$  in the y direction. The diffracted electric field is poloidal (solid lines) whereas the corresponding magnetic field is toroidal (dashed lines).

FIG. 3. Radiation and polarization diagrams of the field diffracted by a magnetic dipole (far-field). The result is the same as for a point anomaly in magnetic permeability. This time the diffracted electric field is toroidal (solid lines) whereas the corresponding magnetic field is poloidal (dashed lines).

FIG. 4. Radiation and polarization diagrams of an impedance anomaly alone.

FIG. 5. Radiation and polarization diagrams of a velocity anomaly alone.

FIG. 6. Synthetic view of the radiation and polarization diagrams of an electric anomaly alone. The solid (resp. dashed) vectors have the direction and amplitude of the electric (resp. magnetic) field diffracted by a point anomaly in electric parameters alone, when illuminated by an electric field  $E_i$ , and its associated magnetic field  $B_i$ .

FIG. 7. Synthetic view of the radiation and polarization diagrams of a magnetic anomaly alone. The solid (resp. dashed) vectors have the direction and amplitude of the electric (resp. magnetic) field diffracted by a point anomaly in magnetic per-

meability alone, when illuminated by an electric field  $E_i$ , and its associated magnetic field  $B_i$ .

FIG. 8. The radiation pattern of antennae used for Figure 9 in the plane perpendicular to the antennae and using normalized amplitude.

FIG. 9. Theoretical signal for a small dipole of frequency 600 MHz, for a CMP type acquisition over a small anomaly of iron-bearing sand, buried two meters deep in dry sand. Top: the total electric field; bottom left: the contribution of the effective velocity contrast; bottom right: the contribution of the effective impedance contrast.

FIG. 10. Peak to peak amplitude of the envelope of the simulated data shown on Figure 9.

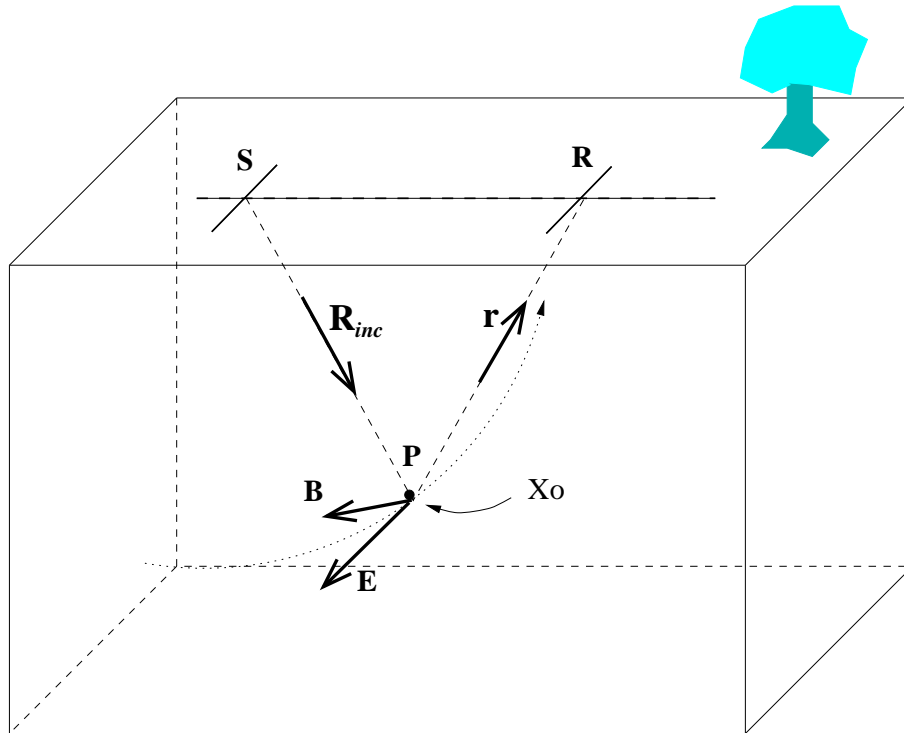
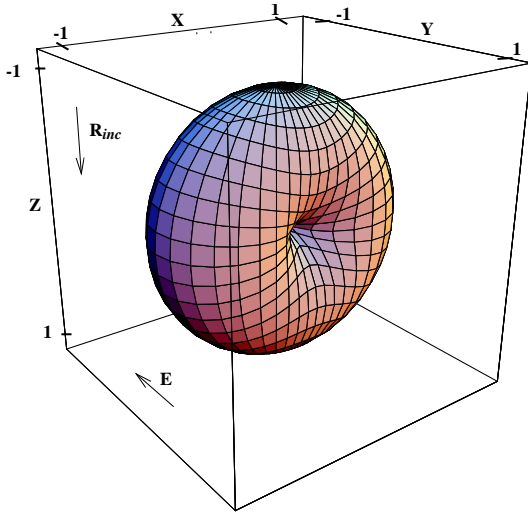


FIG. 1. Position of the antennae and polarization of incident electromagnetic fields on point P.

Radiation Pattern



Polarization Pattern

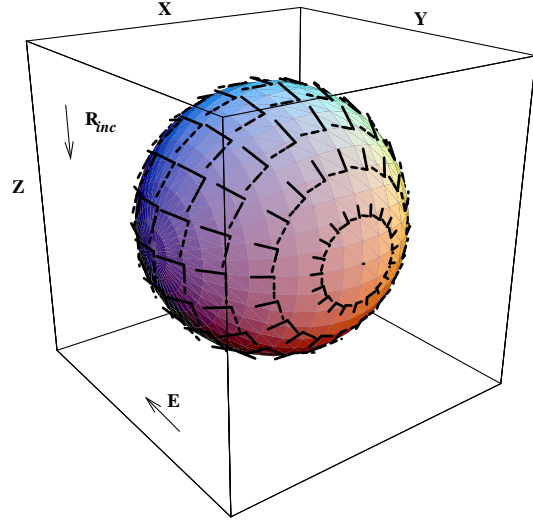
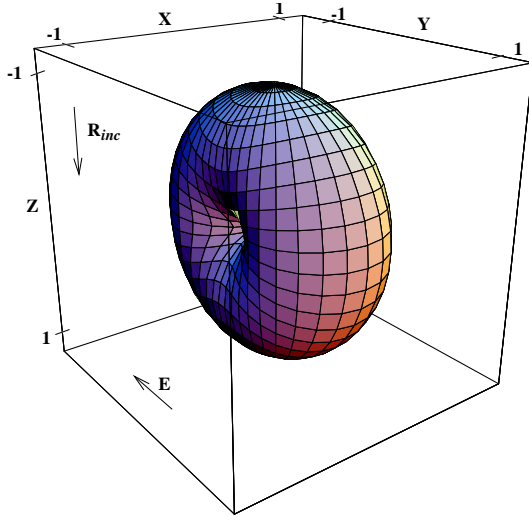


FIG. 2. Radiation and polarization diagrams of an electric dipole, i.e., intensity, direction, and sense of the field diffracted by a point anomaly in electric permittivity alone, or, electric conductivity alone when illuminated by an electromagnetic wave moving in the  $R_{inc}$  direction with an electric field  $\mathbf{E}$  in the  $y$  direction. The diffracted electric field is poloidal (solid lines) whereas the corresponding magnetic field is toroidal (dashed lines).

Radiation Pattern



Polarization Pattern

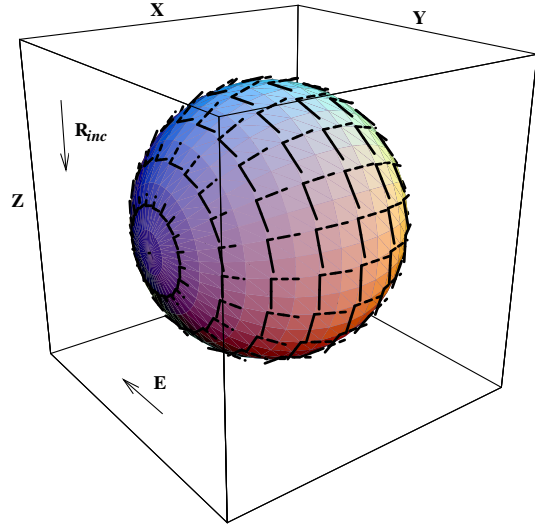
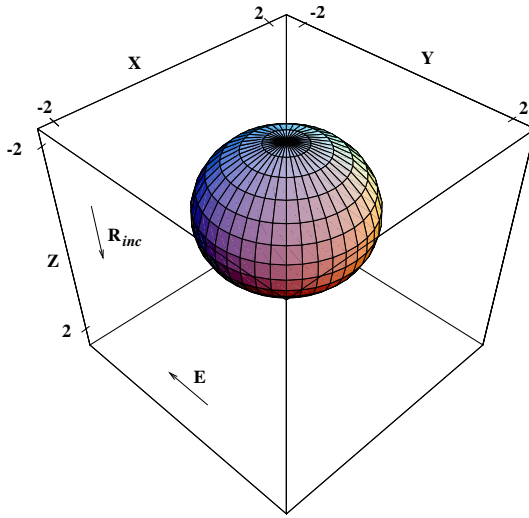


FIG. 3. Radiation and polarization diagrams of the field diffracted by a magnetic dipole (far-field). The result is the same as for a point anomaly in magnetic permeability. This time the diffracted electric field is toroidal (solid lines) whereas the corresponding magnetic field is poloidal (dashed lines).

Radiation Pattern



Polarization Pattern

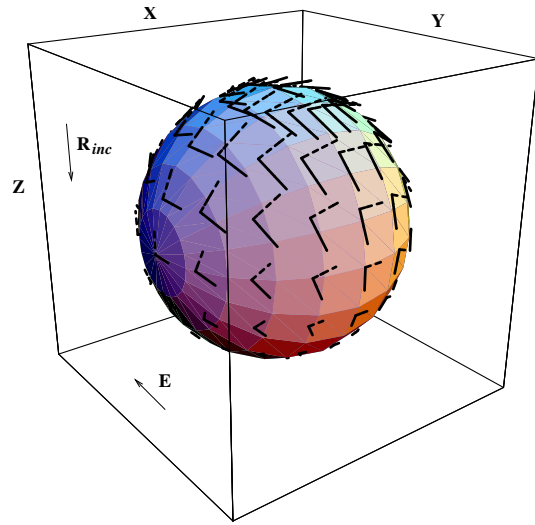
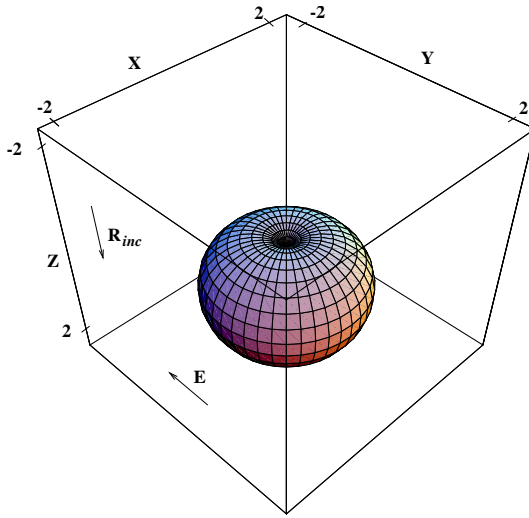


FIG. 4. Radiation and polarization diagrams of an impedance anomaly alone.

Radiation Pattern



Polarization Pattern

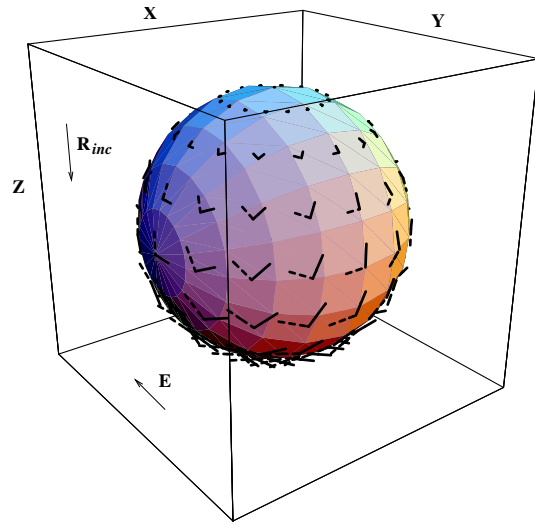


FIG. 5. Radiation and polarization diagrams of a velocity anomaly alone.

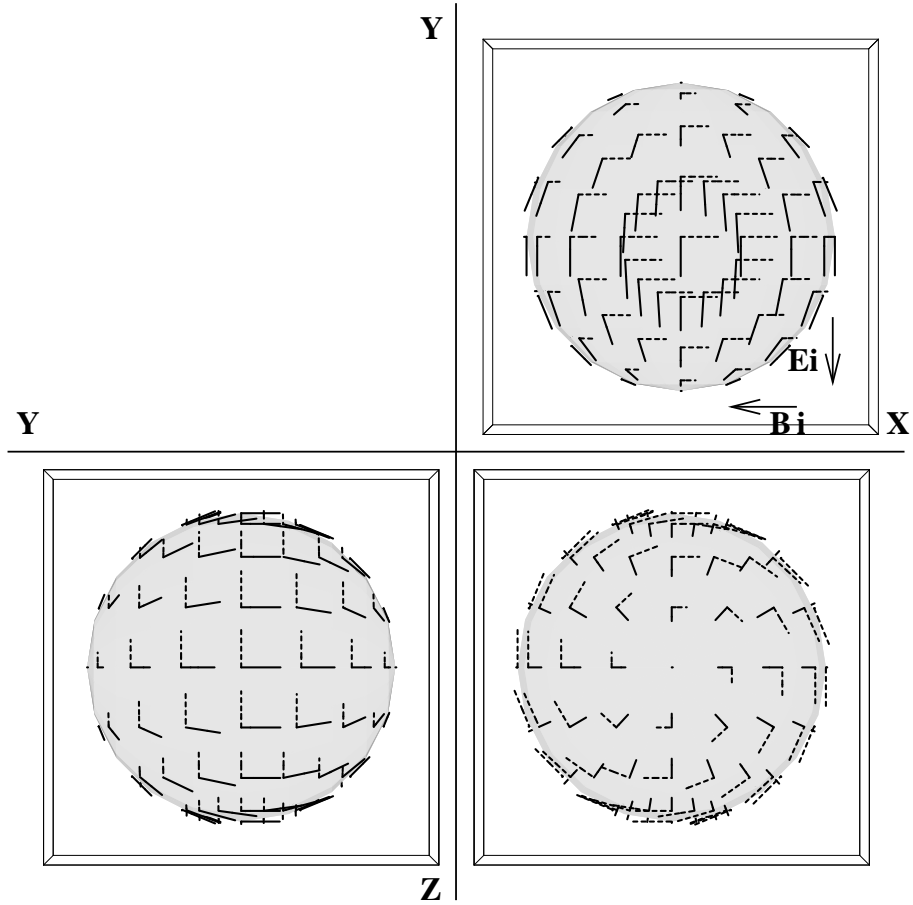


FIG. 6. Synthetic view of the radiation and polarization diagrams of an electric anomaly alone. The solid (resp. dashed) vectors have the direction and amplitude of the electric (resp. magnetic) field diffracted by a point anomaly in electric parameters alone, when illuminated by an electric field  $E_i$ , and its associated magnetic field  $B_i$ .

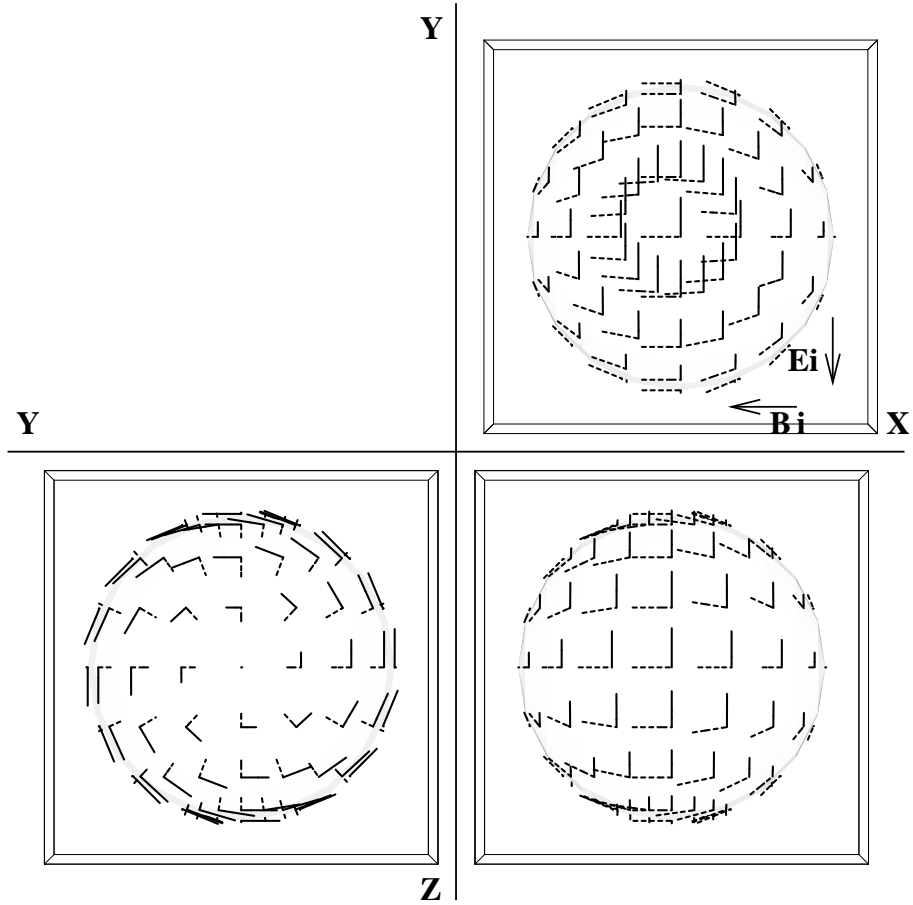


FIG. 7. Synthetic view of the radiation and polarization diagrams of a magnetic anomaly alone. The solid (resp. dashed) vectors have the direction and amplitude of the electric (resp. magnetic) field diffracted by a point anomaly in magnetic permeability alone, when illuminated by an electric field  $E_i$ , and its associated magnetic field  $B_i$ .

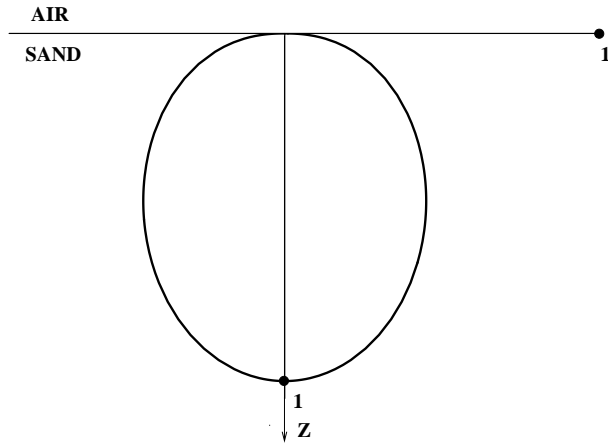


FIG. 8. The radiation pattern of antennae used for Figure 9 in the plane perpendicular to the antennae and using normalized amplitude.

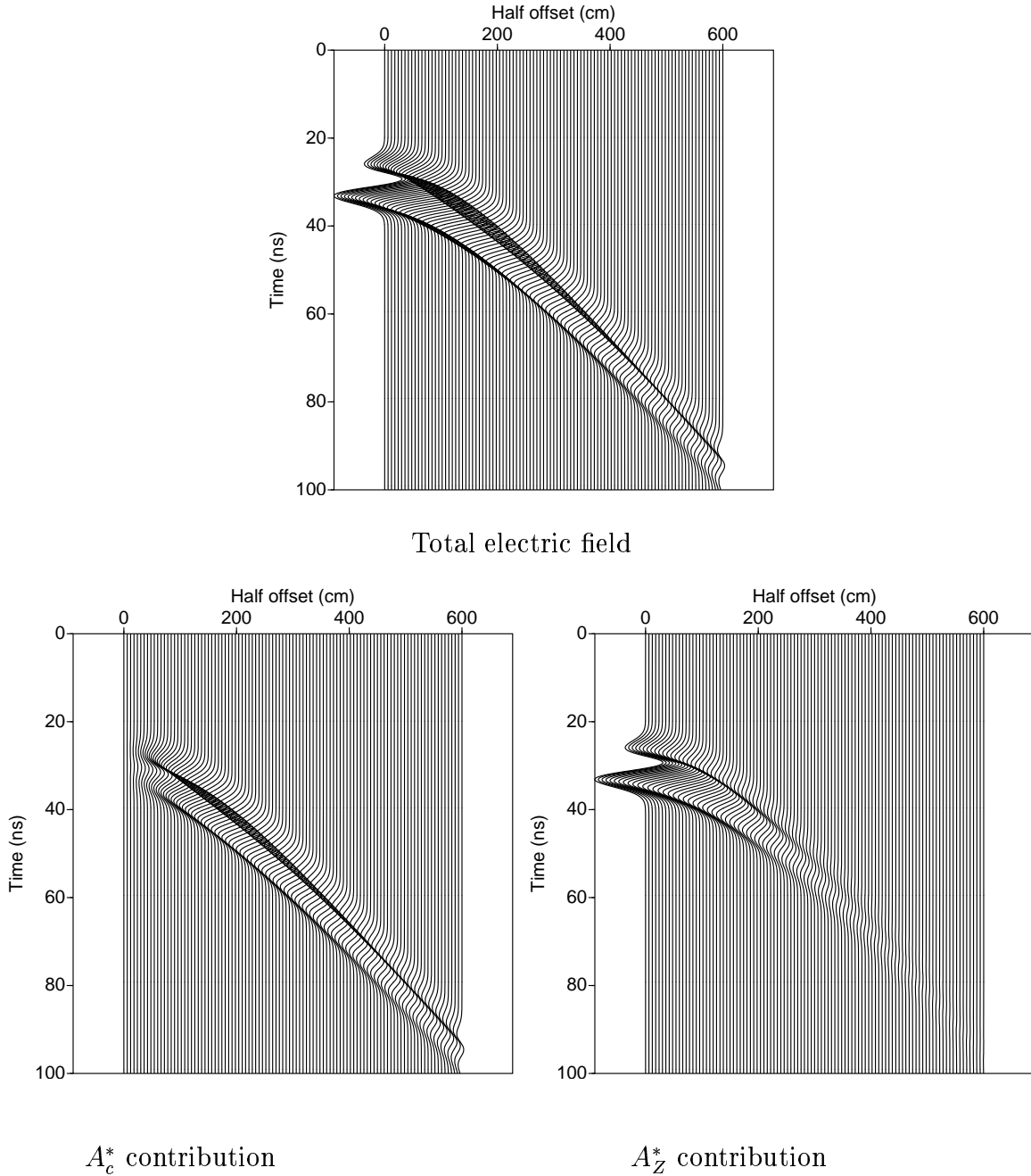


FIG. 9. Theoretical signal for a small dipole of frequency 600 MHz, for a CMP type acquisition over a small anomaly of iron-bearing sand, buried two meters deep in dry sand. Top: the total electric field; bottom left: the contribution of the effective velocity contrast; bottom right: the contribution of the effective impedance contrast.

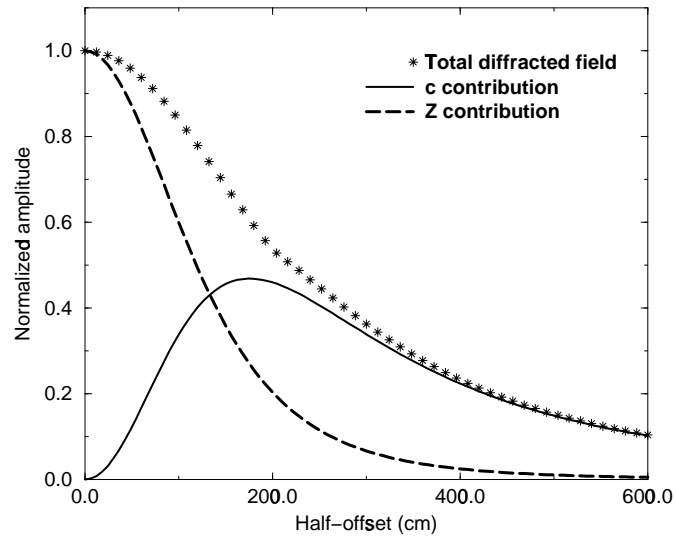


FIG. 10. Peak to peak amplitude of the envelope of the simulated data shown on Figure 9.